CHAPTER 6

STRUCTURAL, DELECTRIC AND IMPEDANCE SPECTROSCOPIC STUDIES ON Fe DOPED $BaTiO_3$

6.1 Introduction

It is known that addition of iron promotes formation of hexagonal $BaTiO_3$ (h-$BaTiO_3$) at relatively lower temperatures [Jaffe et. al. (1971)]. Therefore Fe doped $BaTiO_3$ usually possesses both tetragonal as well as hexagonal phases whose ratio depends upon the amount of Fe doping [Qiu et. al. (2010); Deka et. al. (2014); Dang et. al. (2015); Kolodiazhnyi (2008)]. Substituting more than 10% Fe at Ti site leads to fully hexagonal $BaTiO_3$. The possible technological applications of this system would thus depend upon the overall properties resulting from different phases and their interactions.

In order to produce these materials having properties desired for various applications and develop an understanding of the processes involved , the contributions from the tetragonal and hexagonal phases must be separated out for which impedance spectroscopic studies are very promising [Macdonald et. al. (2005)]. Impedance spectroscopy has been utilized in Fe- doped $BaTiO_3$ to study tetragonal- cubic solid solutions [Maso et. al. (2006)] , grain – grain boundary behaviour in single phase [Sitko et. al. (2015)], NTC behaviour in single phase hexagonal $BaTiO_3$ [Xue et. al. (2012)]. To the best of our knowledge no work has been done on impedance spectroscopic studies of Fe doped BaTiO3 possessing coexisting tetragonal and hexagonal phases.

In this chapter synthesis of $BaTi_{1-x}Fe_xO_3$ with x = 0.03, 0.05, 0.10 by solid state reaction method and its characterization by using XRD , SEM, dielectric and impedance measurements in the frequency range 20 Hz to 1MHz at different

temperatures (300 K - 650 K) are presented . The results are discussed to understand the dielectric behaviour. Using the impedance data in the frequency range 20 Hz – 1 MHz , equivalent circuit models comprising resistive and capacitive components representing the data well have been developed that successfully separates out the contributions from the tetragonal and hexagonal phases. Dielectric permittivity was also measured at microwave frequencies (8 – 12 GHz) at room temperature.

6.2 Experimental

Fe doped $BaTiO_3$ ($BaFe_xTi_{1-x}O_3$, x = 0.03, 0.05 and 0.10 designated as BFT3 , BFT5 and BFT10 respectively) samples were prepared by solid state synthesis technique using $BaCO_3$ (Merck 99.5%), Fe_2O_3 (Merck 99.5%) and TiO_2 (Merck 99.5%). Appropriate amounts of these materials were weighed and mixed in acetone medium for 6 hours. The mixtures were then calcined at 1100 ^{0}C for 6 hours. The calcined powders were ground and mixed with small amount of PVA binder and pressed into disc-like (dia 12 mm, thickness 1.5 mm) and rectangular (23 mm x 10 mm x 4 mm) pellets using uniaxial hydraulic press under 60 kN load. These pellets were sintered in an electrical furnace (Lenton, Germany). Binder was removed by raising the temperature to 500 °C at 2 ºC/min and holding there for 2 hours. Then the temperature was raised to 1250 ºC at 5 ºC/min and held for 10 hours followed by furnace cooling to room temperature.

Phase formation was confirmed by recording room temperature powder X-ray diffraction (XRD) patterns of the calcined and sintered powders using a Rigaku high resolution X-ray diffractometer employing Cu $K_{\alpha 1}$ radiation with Ni-filter in the diffraction angle (2θ) range 20º- 90º using a slow scan rate. Rietveld refinement was carried out using Fullprof software. Surface morphology was studied by Scanning Electron Microscope (ZIESS). For this, one side of the sintered pellets were polished

using emery papers of grade 1/0 (40 μm), 2/0 (30 μm), 3/0 (20 μm) and 4/0 (10 μm) (Sia, Switzerland). The fine polishing was done on blazer cloth using 0.25 μm diamond paste of grade 1/4-OS-475 (HIFIN). The pellets were then thermally etched at 100 ^{0}C lower than the sintering temperature for about 15 minutes to delineate the morphology. The etched pellets were then gold coated.

The dielectric and impedance measurements were carried out using Novocontrol Alpha-A Analyzer in the frequency range 20 Hz to 1 MHz and from 300 K to 650 K. For this the disc like cylindrical pellets were polished using emery papers of grade 1/0 and 2/0 and electroded on both sides using silver paste and cured at 600 ^{0}C for 15 minutes. The high frequency dielectric measurements were carried out at room temperature in X-Band (8.2 GHz – 12.4 GHz) using the Keysight E5071C Network Analyzer. The rectangular pellets were placed in the X-Band rectangular waveguide which was connected to the Network Analyzer through a coaxial cable using a coaxial to waveguide adapter. The measurement technique is based on the so-called transmission line method (Nicolson-Ross-Weir method) which involves placing the sample inside a portion of an enclosed transmission line (in the present system, metallic rectangular waveguide) and measuring scattering parameters S_{11} and S_{21} which are used to obtain the dielectric properties of the material [Nicolson et. al. (1970); Weir (1974)]. The details have been mentioned in section 3.2.5 of chapter 3 and Appendix A.

6.3 Results and Discussion

6.3.1 Phase analysis

X-Ray diffraction patterns for $BaFe_xTi_{1-x}O_3$ (x = 0.03, 0.05 and 0.10) are shown in Figure 6.1. These patterns show that the compositions contain tetragonal and hexagonal phases simultaneously. The amount of these phases is strongly influenced by the level of Fe doping. The hexagonal and tetragonal phases match with the JCPDS code 82-1175 (space group P63/mmc) and 79-2264 (space group P4mm) respectively. It is evident from the observations of the dominant peaks (Figure 6.1(b)) of both the phases, namely 104(hexagonal) and 101(tetragonal) that composition with x=0.03 contains small amount of hexagonal phase whereas the composition with x=0.05 contains both the phases in nearly equal amount. In the sample with x=0.10, the tetragonal phase becomes very small. It is known that the processing parameters such as atmosphere during heat treatment, temperature and/or duration of sintering affect the growth of phases .That is why various research groups report different findings on the phase formation of Fe doped $BaTiO_3$. While Lin et al. (2008) report pure hexagonal phase formation for x > 0.10, Rajan et al. (2016) report a combination of tetragonal and cubic phases for x=0.005. Xu et al. (2009) and Khirade et al. (2016) claim pure tetragonal phase formation for x=0.05 and x=0.10 respectively. Our finding of the presence of a mixture of hexagonal and tetragonal phases is in agreement with the results reported by Qiu et al. (2010) (for $0 \leq x \leq 0.10$), Deka et al. (2014) (for $x \geq 0.10$), Rani et. al. (2016) (for $0 \leq x \leq 0.10$), and Dang et. al. (2015) (for $0 \leq x \leq 0.12$). 6H–$BaTiO_3$ polymorph is thermodynamically stable above 1460 ^{0}C [Dang et. al. (2015); Nguyen et al. (2011); Xue et al. (2012)]. Our XRD results show that Fe doping leads to the kinetic stabilization of 6H–$BaTiO_3$ phase at room temperature and a decrease in its formation temperature down to 1250 ^{0}C.

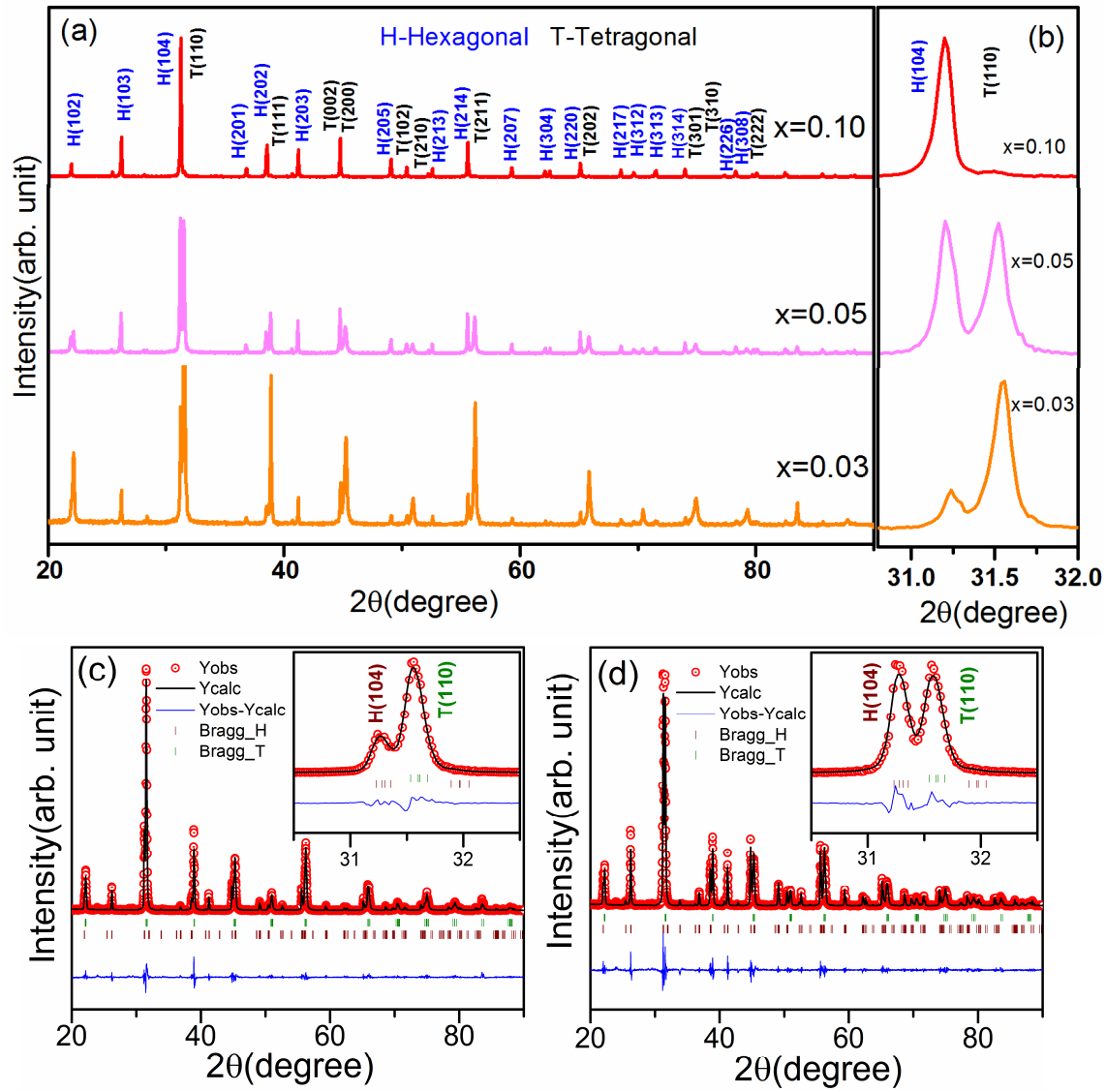

Figure 6.1: (a) XRD patterns of $BaFe_xTi_{1-x}O_3$ (x = 0.03, 0.05 and 0.10), (b) Magnified peaks near 31.5 degree , where the right hand side peak corresponds to tetragonal phase (c) Rietveld refinement for x=0.03. Inset: magnified peaks around 31.5 degree. (d) Rietveld refinement for x=0.05. Inset: magnified peaks around 31.5 degree.

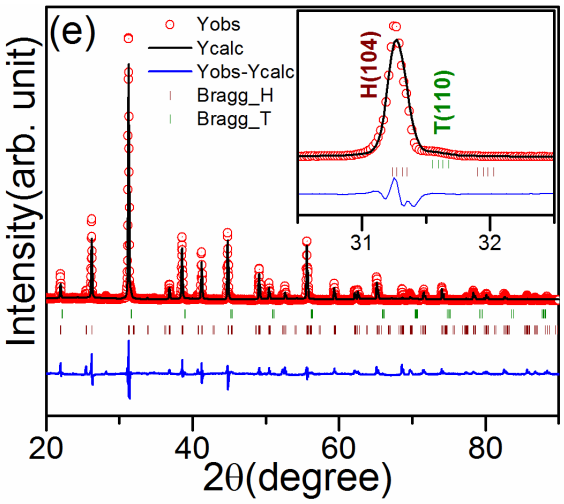

Figure 6.1(contd.): (e) Rietveld refinement of x=0.10. Inset: magnified peaks around 31.5 degree.

Formation of almost entirely hexagonal phase for x = 0.10 is in agreement with Keith et al. (2004) who have reported room temperature stabilized hexagonal phase for 0.10 ≤ x ≤0.50.

Rietveld refinement of the XRD data was carried out using Fullprof software. Figures 6.1(c-e) show the same with insets depicting the H(104) and T(110) peaks around $2\theta=31.5^0$. The lattice parameters (a, c) and unit cell volume (V) of the tetragonal and hexagonal phases for x = 0.03, 0.05 and 0.10 are given in Table 6.1 along with Rietveld parameters. It is observed that there is an increase in the tetragonal lattice parameter 'a' and decrease in 'c' in comparison with P4mm space group JCPDS file 79-2264. The hexagonal lattice parameter 'a' decreases and 'c' increases in comparison with P63/mmc space group JCPDS file 82-1175. The hexagonal unit cell volume (V) also increases with increase of Fe content. This can be due to substitution of Ti^{+4} ions (ionic radius r_i=0.605 Å) by bigger Fe^{+3} ions (ionic radius r_i = 0.645 Å) [Deka et al. (2014); Khirade et al. (2016); Rani et al. (2016)]. It is interesting to observe that while the c/a ratio as well as the unit cell volume (V) for the hexagonal phase increases with Fe content, the tetragonal phase exhibits an opposite trend.

Table 6.1: Fitted cell parameters and figure of merits for the compositions x=0.03, 0.05 And 0.10 where Ref 1 and Ref 2 correspond to JCPDS 79-2264 and JCPDS 82-1175 respectively.

x	Tetragonal Phase				Hexagonal Phase				S	χ^2
	a(Å)	c(Å)	c/a	V(Å)^3	a(Å)	c(Å)	c/a	V(Å)^3	(R_{wp}/R_e)	
Ref1	3.9998	4.0180	1.0045	64.280	-	-	-	-	-	-
Ref2	-	-	-	-	5.7238	13.9649	2.4397	396.220	-	-
0.03	4.0006	4.0174	1.0041	64.301	5.7239	13.9866	2.4435	396.644	1.64	2.76
0.05	4.0006	4.0149	1.0035	64.258	5.7229	13.9872	2.4440	396.737	1.64	2.65
0.10	4.0010	4.0124	1.0028	64.232	5.7216	13.9950	2.4459	396.779	1.73	3.57

6.3.2 Microstructure and Energy Dispersive Spectroscopy

Scanning Electron Micrographs are given in Figure 6.2(a,c,e) with their corresponding Energy Dispersive Spectroscopy (EDS) spectra in Figure 6.2(b,d,f). It is seen that the average grain size increases with amount of Fe doping which can be due to development of an inter-granular interaction that leads to merging of grains [Rajan et al. (2016)]. It is noticed that for x=0.03, the grains are almost spherical, for x=0.05 some rod-like or rectangular grains appear and for x=0.10 most of the grains are rod-like.

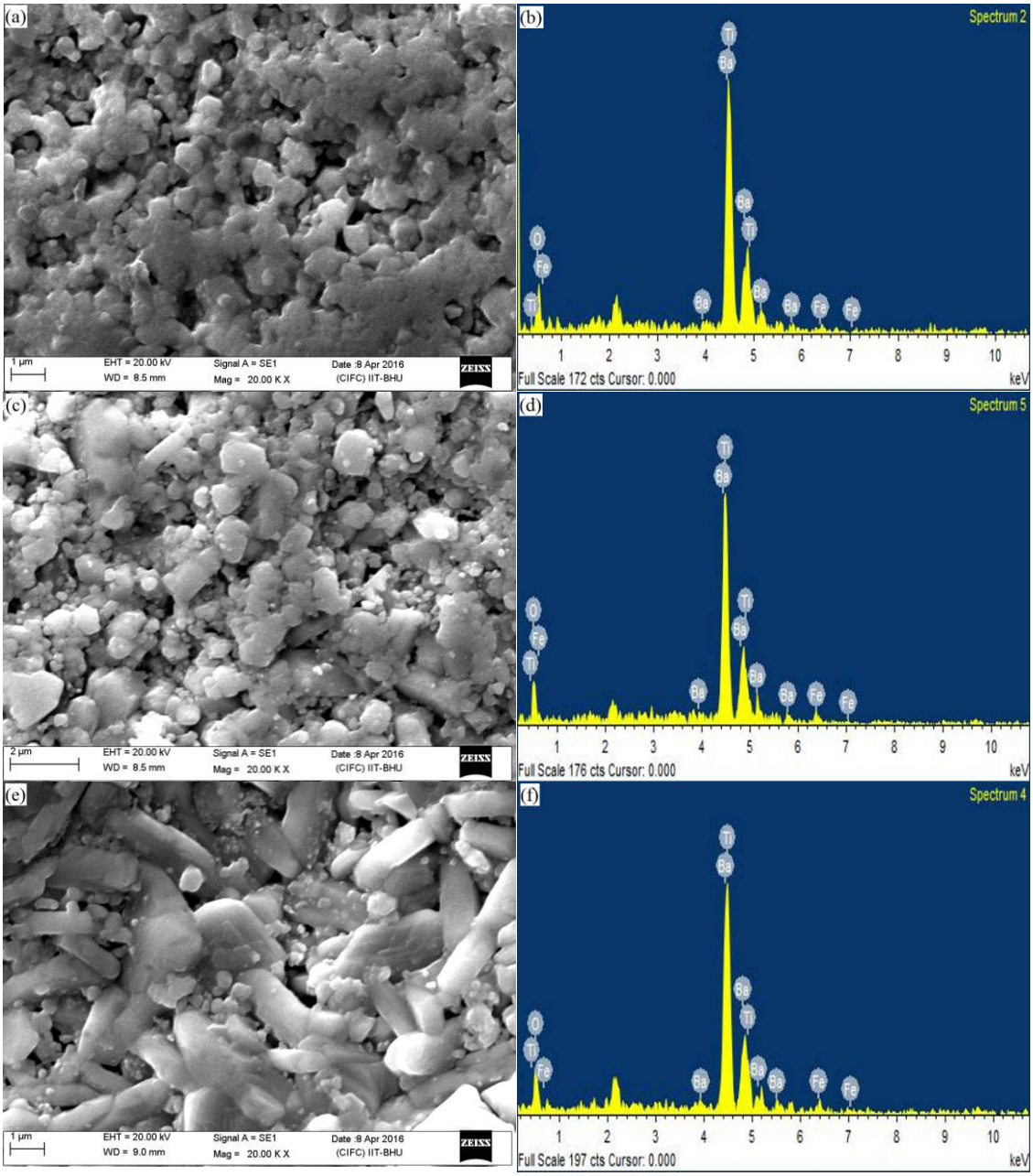

Figure 6.2: SEM micrographs and EDS spectra for $BaFe_xTi_{1-x}O_3$ (a,b) x=0.03, (c,d) x=0.05, and (e,f) x=0.10 samples.

It implies that the fraction of hexagonal phase increases with level of Fe doping. This is also supported by XRD patterns shown in Figure 6.1. It seems that grains are somewhat agglomerated, presumably due to longer dwell time (~10 hrs) during sintering.

The EDS spectra shown in Figure 6.2 (b,d,f) clearly depict the presence of Ba^{2+} (4.46 keV), Fe^{3+}(0.7 and 6.39 keV), Ti^{4+}(0.45 and 4.5 keV) and O^{2-}(0.52 keV) elements. [Khirade et al.(2016)]. Table 6.2 presents the weight and atomic fractions obtained from EDS that support the presence of above elements as expected from the initial composition.

Table 6.2: EDS results for compositions x = 0.03, 0.05 and 0.10.

Composition	Ba		Ti		Fe		O	
	Wt %	**At%**	**Wt %**	**At%**	**Wt %**	**At%**	**Wt %**	**At%**
x=0.03	58.87	20.06	19.84	19.34	0.77	0.64	20.51	59.96
x=0.05	58.75	19.96	19.51	19.04	1.25	1.06	20.49	59.94
x=0.10	58.61	19.93	18.49	18.07	2.44	2.07	20.46	59.93

6.3.3 Dielectric characterization (RF Range)

Variation of permittivity (ε′) and dielectric loss as a function of temperature (T) at various frequencies for x = 0.03, x = 0.05 and x = 0.10 are shown in Figures 6.3, 6.4 and 6.5 respectively. It is noted from Fig. 6.3(a) that ε′ exhibits a broad maxima around 370 K at 1 kHz. The peak temperature shifts to higher side with increasing frequency. A strong frequency dependence of ε′ is observed near peak temperature. A peak is also observed in the corresponding dielectric loss vs temperature plots in Figures 6.3(c). The peak temperature shifts to higher side with increasing frequency in this case also. These features show that this composition mimics ferroelectric relaxor behavior.

A very broad and diffuse peak is observed around 373 K without any observable frequency dependence of the peak temperature (T_m) for x= 0.05 (Figures 6.4 (a)). The

maximum value of permittivity (ε'_m) for the samples is much less than that of pure $BaTiO_3$ [Xu et al. (2009)]. This may be due to substitution of Ti^{4+} ions with less polarisable Fe^{2+} and Fe^{3+} ions [Xu et al. (2009); Rani et al. (2016)]. From the permittivity vs. frequency graph (Figure 6.4(b)) it is evident that the permittivity decreases rapidly up to 10 kHz after which it remains almost constant up to 1 MHz. The rapid decrease in the permittivity up to 10 kHz may be attributed to the interfacial polarization or space charge polarization. Interfacial polarization arises due to presence of two phases, viz. tetragonal and hexagonal, having different conductivity. At higher frequencies (above 10 kHz for x=0.03 and 100 kHz for x=0.05) the permittivity remains nearly constant. This may be due to relaxation of space charge polarizations in fast varying electric field at higher frequencies. The dielectric permittivity for x = 0.05 is higher than that of x = 0.03 throughout the frequency range from 100 Hz to 1 MHz (Figure 6.4). This may be due to larger number of hexagonal grains in the x = 0.05 sample than in x = 0.03 sample. This would lead to enhanced contact regions and hence interfacial polarization between tetragonal grains and hexagonal grains as mentioned.

A broad peak is also observed for x = 0.10 around 500 K having frequency dependence of the peak temperature (T_m) (Figure 6.5 (a)). Its room temperature value of ε' (153 at 1 KHz) is much lower than those for x = 0.03 and 0.05. This may be due to the fact that the composition x = 0.10 contains almost entirely hexagonal phase.

It is known that doping of Fe in $BaTiO_3$ leads to broadening of ferroelectric phase transition peak [Mishra et al. (2012); Dutta et al. (2016); Maso et al. (2006); Rajan et al. (2016)]. The profile of the ε' as a function of temperature (T) curves for the samples x = 0.03 and x = 0.05 show similar broadening. To understand the nature of this broadening $1/\varepsilon'$ vs T was fitted in accordance with the Curie-Weiss law given below (Equation (6.1))

$$1/\varepsilon' = C/(T-T_C) \qquad \ldots(6.1)$$

where C is Curie constant(K^{-1}) and T_C is Curie Temperature (K).

In both the samples, the data deviated from the Curie-Weiss law as shown in the Figure 6.6. This is in agreement with the results reported earlier and indicates the presence of diffuse phase transition (DPT) [Maso et al. (2006)]. By using the high temperature linear portion of the graphs (for x=0.03 and 0.05) and a linear fit, the temperature at which the deviation starts (the so-called Burn's temperature, T_B) was obtained as indicated by dotted line in Figure 6.6. The degree of diffuseness was estimated by fitting the experimental data to the modified Curie-Weiss law (Equation (6.2)) [Uchino et al. (1982)]

$$1/\varepsilon' - 1/\varepsilon'_m = (T-T_m)^{\gamma} / C, \qquad (T > T_m) \qquad \ldots(6.2)$$

where ε'_m is the maximum permittivity and T_m is the corresponding temperature and γ is diffusivity parameter.

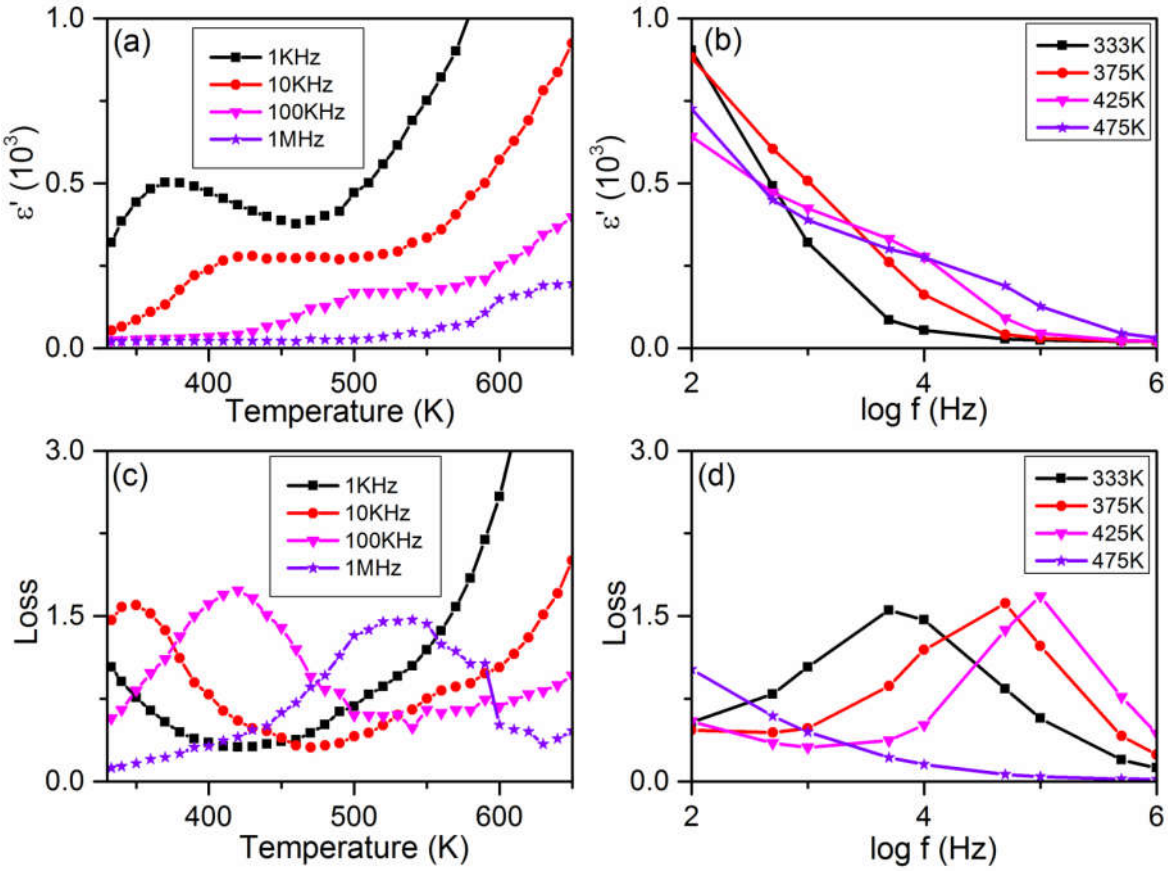

Figure 6.3: $BaFe_xTi_{1-x}O_3$ (x = 0.03) plots for (a) Permittivity (ε′) vs. Temperature for various frequencies (b) Permittivity (ε′) vs. log f for various temperatures (c) Dielectric loss vs. Temperature for various frequencies (d) Dielectric loss vs. log various temperatures

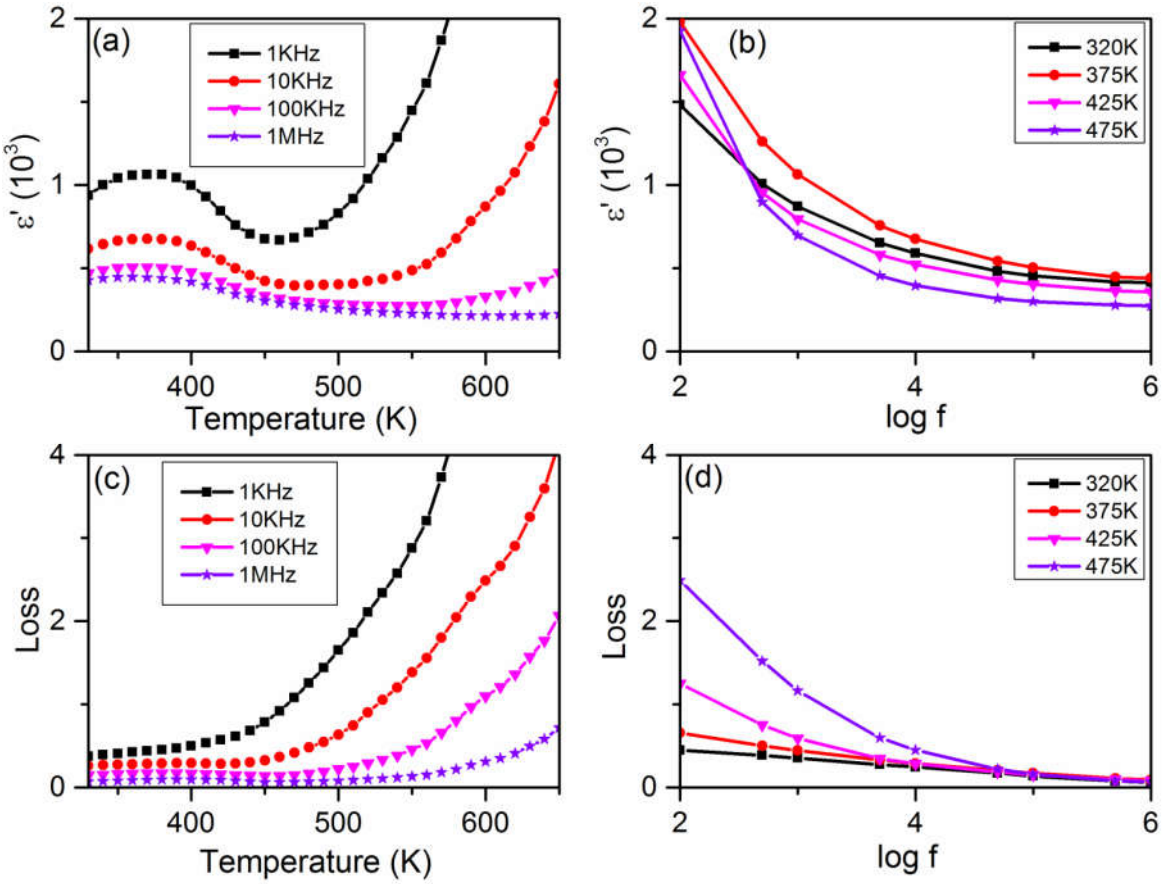

Figure 6.4: $BaFe_xTi_{1-x}O_3$ (x = 0.05) plots for (a) Permittivity (ε′) vs. Temperature for various frequencies (b) Permittivity (ε′) vs. log f for various temperatures (c) Dielectric loss vs. Temperature for various frequencies (d) Dielectric loss vs. log f for various temperatures

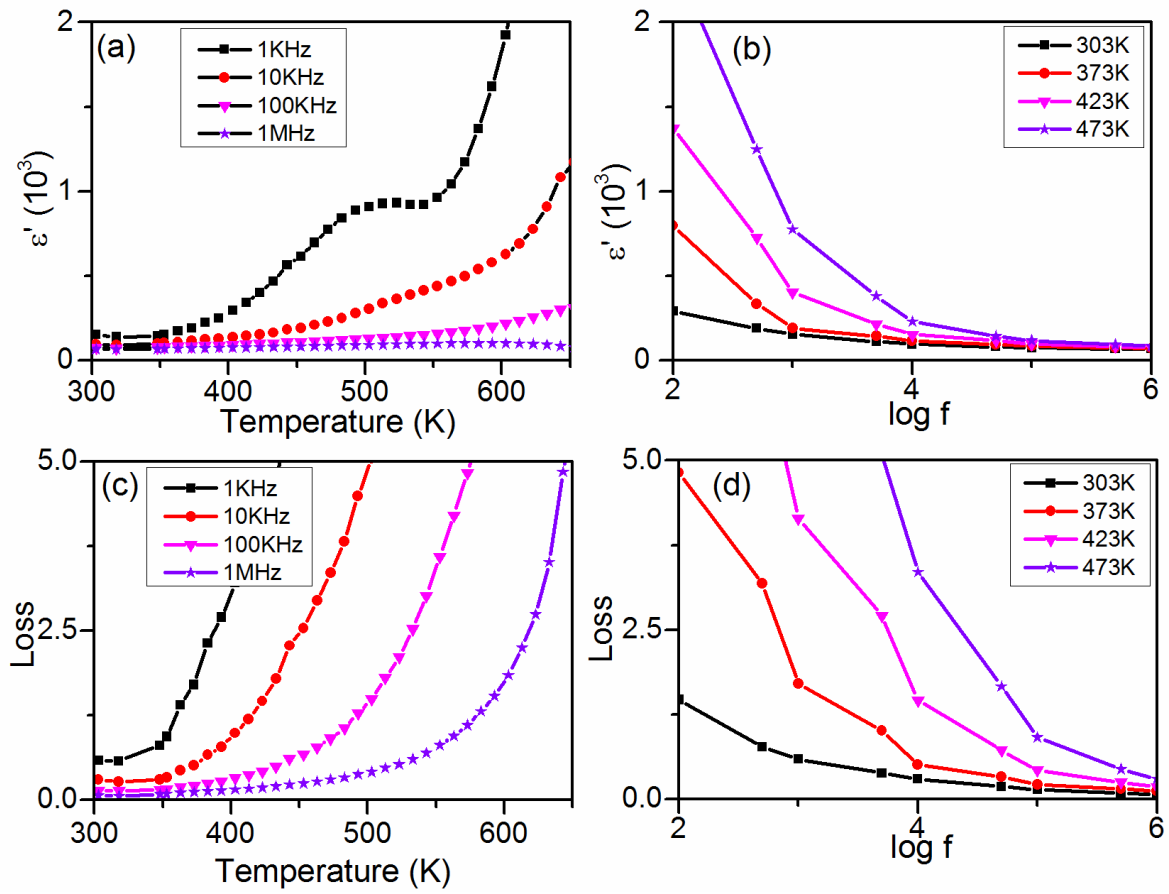

Figure 6.5: $BaFe_xTi_{1-x}O_3$ (x = 0.10) plots for (a) Permittivity (ε′) vs. Temperature for various frequencies (b) Permittivity (ε′) vs. log f for various temperatures (c) Dielectric loss vs. Temperature for various frequencies (d) Dielectric loss vs. log f for various temperatures.

Here γ = 1 corresponds to normal ferroelectric phase transition, γ = 2 to the so called complete relaxor while 1< γ < 2 indicates Diffuse Phase Transition (DPT). The values of γ were obtained by fitting the experimental values of $\ln(1/\varepsilon' - 1/\varepsilon'_m)$ vs $\ln(T-T_m)$ plots in accordance with Equation (6.2) in the temperature range T_m to T_B (Inset of Figures 6.6 (a, b)). The best fit values for ε'_m, T_m, γ and C were obtained at 1 kHz and are given in Table 6.3. It may be mentioned that displacive ferroelectrics such as barium titanate exhibit Curie constant of the order of 10^5. Higher order values of Curie constant are a signature of DPT [Xue et al. (2012)]. The value of γ calculated above indicate that sample with x = 0.05 should exhibit relaxor behaviour whereas that with x = 0.03 should exhibit DPT behavior. Value of γ for x=0.03 is 1.22 which is much less than 2,

a feature characteristic of DPT. It is observed that value of γ~2 obtained for x=0.05 indicates that this composition should exhibit ferroelectric relaxor behavior. But ε′ vs T plots in Figure 6.4(a) show that peak temperature does not depend on frequency which is also a characteristic feature of DPT. On the other hand in the composition with x=0.03 the peak temperature shifts with frequency of measurement, a characteristic of ferroelectric relaxors. But the value of γ obtained for this composition is 1.22 (Table 6.3) which points towards DPT. The reason for this unusual behavior is not clear at present. This may be due to co-existence of two phases in these compositions. It may be mentioned that Tsurumi et al. (1994) have proposed mechanism of diffuse phase transition in relaxor ferroelerctrics. They conclude that diffuse phase transition is the result of overlapping phenomenon of volume increase of polar micro regions (PMR), freezing of fluctuating dipoles and dielectric relaxation at measuring frequency. However, they studied single phase systems whereas we are investigating systems having two coexisting phases. Further, all the ε′ vs T plots show a rising trend at higher temperatures which may be due to electrode effects. This may overlap with the peak in ε′ at T_m making it difficult to be clearly visible. Therefore, looking at the data shown in Figure 6.5(a) for x = 0.10, analysis using modified Curie-Weiss law was not possible.

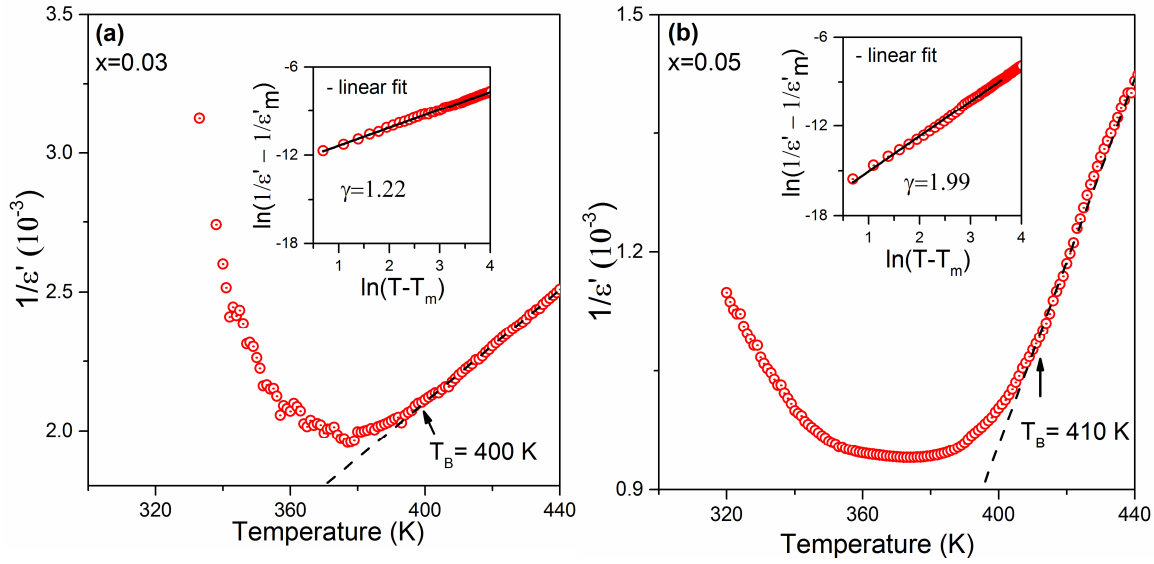

Figure. 6.6: (a) Inverse permittivity vs temperature curve fitted according to Curie-Weiss law for $BaFe_xTi_{1-x}O_3$ (x = 0.03). Inset : $\ln(1/\varepsilon' - 1/\varepsilon'_m)$ vs. $\ln(T-T_m)$ curve fitted according to Modified Curie-Weiss law (b) Inverse permittivity vs. temperature curve fitted according to Curie-Weiss law for $BaFe_xTi_{1-x}O_3$ (x = 0.05). Inset: $\ln(1/\varepsilon' - 1/\varepsilon'_m)$ vs. $\ln(T-T_m)$ curve fitted according to modified Curie-Weiss law.

Table 6.3: The best fit values for ε'_m, T_m, γ and C at 1 kHz for $BaFe_xTi_{1-x}O_3$ (x = 0.03, 0.05) in accordance with modified Curie-Weiss Law (Equation (6.2))

Composition	ε'_m	T_m (K)	T_B (K)	$\Delta T = T_B - T_m$	γ	C (10^6 K^{-1})
x = 0.03	510.8	377	400	23	1.22	0.29
x = 0.05	1063.7	374	410	36	1.99	17.60

6.3.4 Impedance Spectroscopy and Equivalent Circuit Modelling

Complex plane and spectroscopic modulus experimental data were analyzed with a view to separate the grains and grain boundary contributions. Impedance analysis may be carried out by using any of the formalisms viz. impedance $Z^*=Z'-jZ''$, modulus $M^* = M'+jM'' = j\omega C_0 Z^*$, admittance $Y^* = Y'+ jY'' = (Z^*)^{-1}$ and permittivity $\varepsilon^*= \varepsilon'- \varepsilon'' = (j\omega C_0 Z^*)^{-1}$. Here $j = \sqrt{-1}$ and $\omega = 2\pi f$, f being the frequency of the AC excitations used in the measurement and C_0 the capacitance of the empty cell used to house the sample. Preference is given to the formalism which reveals more details and facilitates

separation of different polarization processes [Pandey et al. (1995)]. Also simple model equivalent circuits are chosen to start with to represent the data. In the present study M formalism was found to be more useful.

A parallel RC circuit has one time constant and thus this model circuit is conveniently used to represent one charge transfer process. It is known that M″ vs M′ plot of a parallel RC circuit model is a semicircular arc passing through origin and has a high frequency intercept at C_0/C [Macdonald (2005); Pandey et al. (1995)]. Also appearance of a steeply rising high frequency nonlinear branch in the M″ vs. M′ plot indicates presence of a series resistance in the model. Similarly, appearance of a shift in the M″ vs. M′ plot indicates presence of a series capacitance in the model [Pandey et al. (1995)]. A simple model useful to represent two charge transfer processes would comprise two parallel RC's , say R_1C_1 and R_2C_2, connected in series and would yield a M″ vs M′ plot which would pass through origin and have intercept of $C_0/C_1 + C_0/C_2$ with the M′ axis at high frequency end. For representing presence of more charge transfer processes more RC's are used.

Typical plots of M″ vs M′ , M′ vs log f and M″ vs log f for BFT3 are shown in Figures. 6.7 (a) and (b) for T = 350 K and in Figures. 6.7 (c) and (d) for T = 550 K.

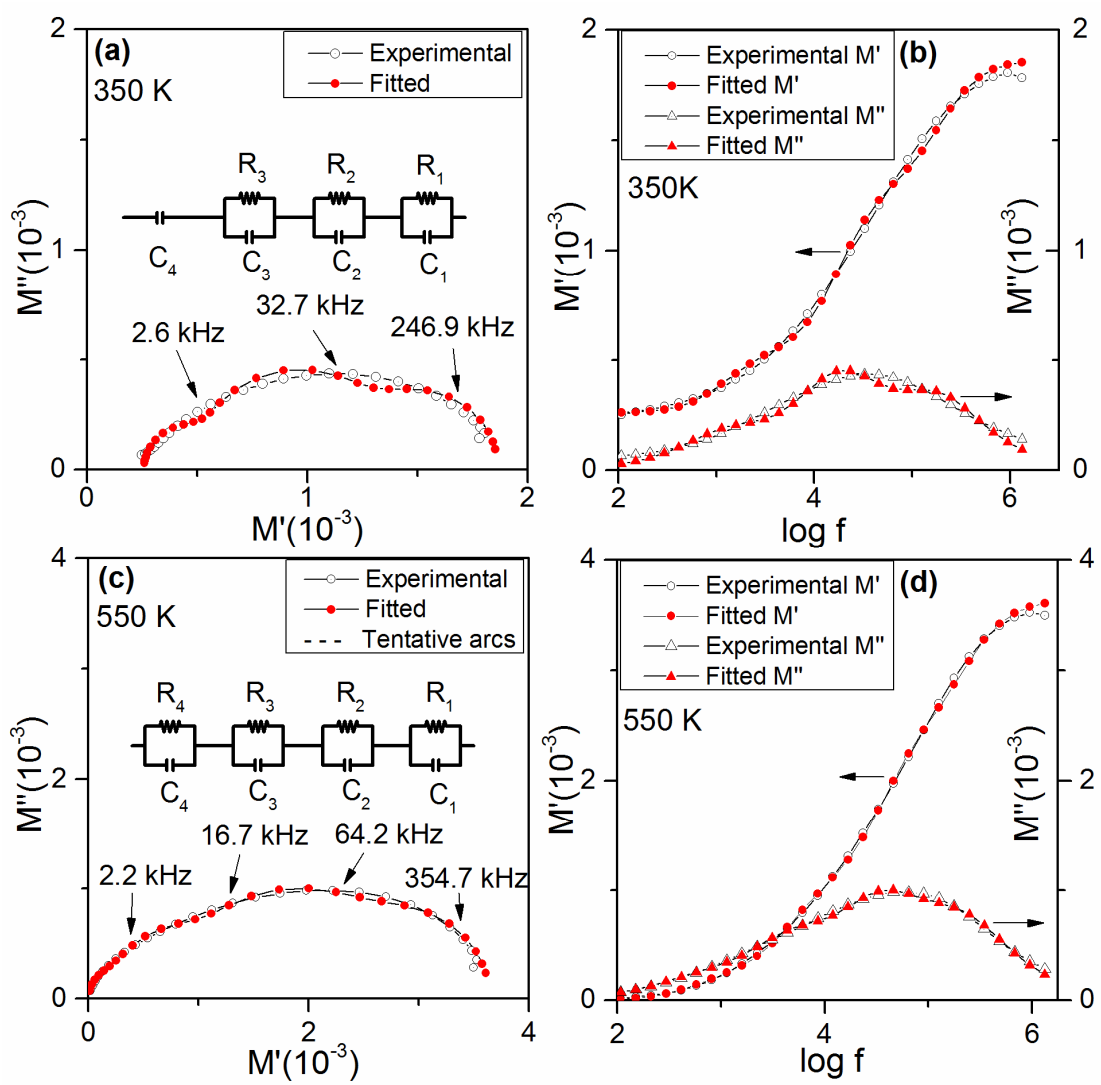

Figure 6.7: Experimental and fitted plots of (a) M″ vs. M′ at 350K (b) M′, M″ vs. log f at 350 K (c) M″ vs. M′ at 550 K and (d) M′, M″ vs. log f at 550 K for $BaFe_xTi_{1-x}O_3$ (x=0.03).

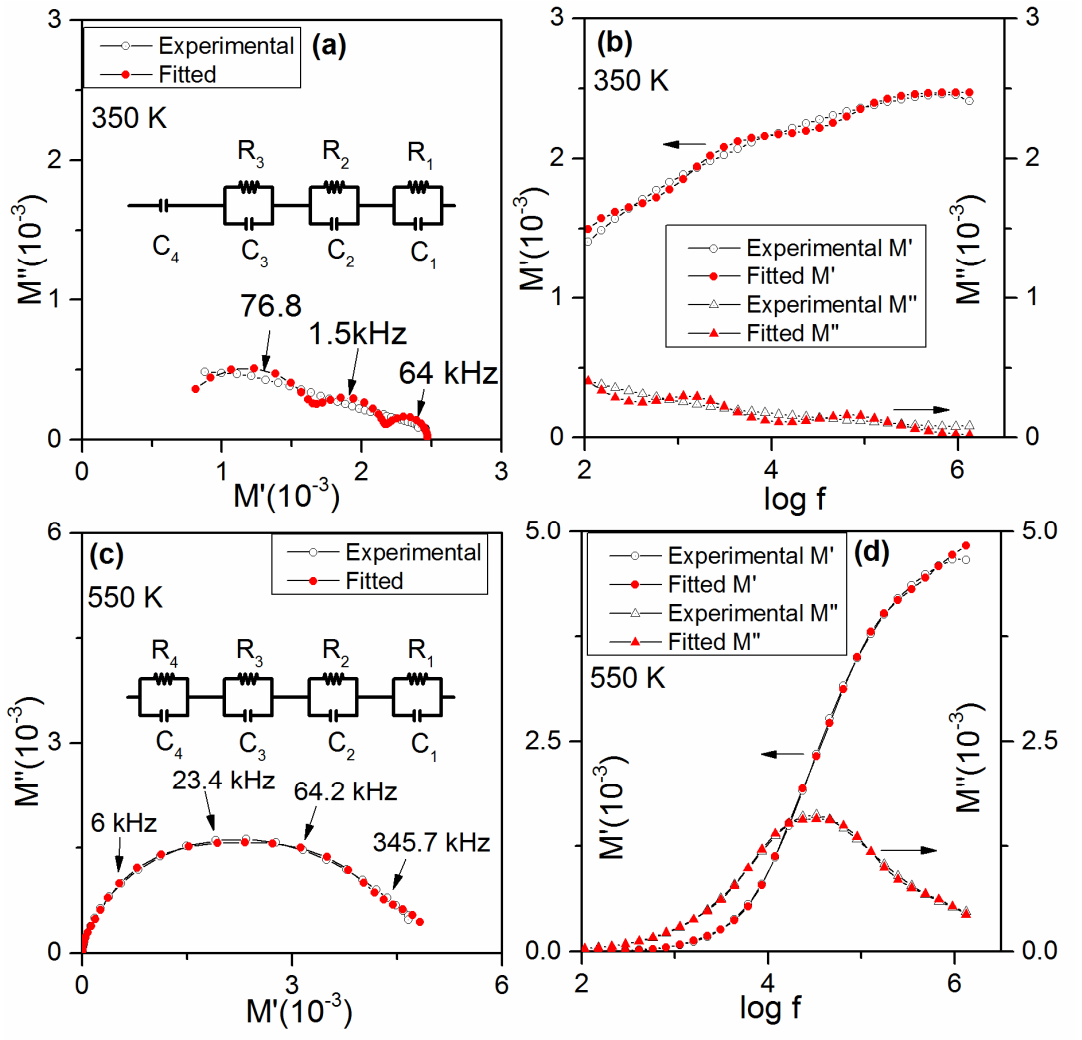

Figure 6.8: Experimental and fitted plots of (a) M″ vs. M′ at 350K (b) M′, M″ vs. log f at 350 K (c) M″ vs. M′ at 550 K and (d) M′, M″ vs. log f at 550 K for $BaFe_xTi_{1-x}O_3$ (x = 0.05)

For convenience we consider plots of Figure 6.7 (c) first. A quick look at the plot reveals that the M″ vs. M′ curve passes through origin, does not have any shift or steeply rising high frequency part and has a high frequency intercept with the M′ axis. Therefore presence of series capacitance or resistance is ruled out. As discussed in the previous sections, the system contains hexagonal as well as tetragonal phases of $BaTiO_3$. The sample - electrode system then comprises the two phases, grain boundary and electrodes. Therefore an equivalent circuit model possessing two parallel RC combinations, say R_1C_1 and R_2C_2, connected in series, representing these phases, further connected to R_3C_3 and R_4C_4 representing grain boundary and contact electrodes respectively, may be used to represent the electrical behavior of the system. The values of the components R_1,C_1,R_2,C_2 etc were estimated by drawing tentative semicircular arcs on the plots representing individual independent contributions from the RC's and by noting the values of the intercepts on the M′ axis and the frequencies where the corresponding arcs peak [Thakur et al. (2004)].

The simulated M″ vs. M′ plot for the model having four RC's in series would have the intercepts of the M″ vs. M′ curve with M′ axis at C_0/C_4, $C_0/C_4 + C_0/C_3$, $C_0/C_4 + C_0/C_3 + C_0/C_2$ and $C_0/C_4 + C_0/C_3 + C_0/C_2 + C_0/C_1$ as the frequency increases from left to right in this plot if it is assumed that the time constants are well separated and are such that $R_1C_1 < R_2C_2 < R_3C_3 < R_4C_4$ [Thakur et al. (2004)]. Thus the arc on extreme left corresponds to R_4C_4 and that on the extreme right corresponds to R_1C_1. The accurate values of these R's and C's were then obtained by fitting the data by a Complex Non Linear Least Squares procedure by taking these values as initial guesses [Macdonald (2005); Thakur et al. (2004)]. The fitted and the experimental values are shown in Figures 6.7 (c,d) in complex plane as well as spectroscopic plots. The plots for

the data for BFT3 in the temperature range 450K-650K are similar as discussed above and were analysed in the same way.

The M″ vs. M′ plots for temperatures below 450 K had a shift towards right. A typical M" vs. M' plot for BFT3 at 350 K is shown in Figure 6.7(a). It does not pass through origin and has a high frequency intercept indicating that the equivalent circuit model would contain a series capacitance and would not contain a series resistance. Therefore a model comprising series combination of parallel R_1C_1, R_2C_2, R_3C_3 further connected to C_4 in series was chosen. As before, R_1C_1 and R_2C_2 were assumed to represent the two phases and R_3C_3 represents the grain boundary. Here C_4 was attributed to the electrode process keeping in mind that a R_4C_4 combination is in fact equivalent to C_4 for extremely large values of R_4. The values of the components were obtained in the same way as described above by first estimating their values from the intercepts of the tentative arcs and then using these as initial guesses in the Complex Nonlinear Least Squares program. The fitted and the experimental values are shown in Figure 6.7(a,b). The values of the components obtained for BFT3 in this way are given in Table 6.4.

The data for BFT5 showed similar behavior and were analyzed in the same way as for the sample BFT3. The plots for BFT5 are shown in Figures 6.8 (a - d). The values of the components(R's and C's) of the equivalent circuit models are given in Table 6.5.

It is seen that values of R_2 are much more than R_1. It has been reported that resistivity of the oxygen deficient hexagonal barium titanate is low and has very weak temperature dependence above 200K [Kolodiazhnyi et al. (2008)]. Therefore R_1 was assigned to the hexagonal phase and R_2 to the tetragonal phase. Thus R_1C_1 and R_2C_2 represent hexagonal and tetragonal phase respectively.

Table 6.4: Values of the components for equivalent circuit model for BFT3 (x = 0.03)

Temp(K)	R_1(KΩ)	C_1(nF)	R_2(KΩ)	C_2(nF)	R_3(KΩ)	C_3(nF)	R_4(KΩ)	C_4(nF)
300	0.64 ±0.02	1.09 ±0.01	14.76 ±0.28	0.838 ±0.01	154.03 ±3.79	1.71 ±0.01	--	3.19 ±0.04
350	1.41 ±0.02	0.91 ±0.01	18.91 ±0.06	0.955 ±0.01	176.43 ±1.30	4.05 ±0.02	--	3.33 ±0.01
400	1.14 ±0.08	1.39 ±0.04	37.94 ±1.44	0.821 ±0.01	283.20 ±14.85	2.31 ±0.08	--	3.33 ±0.09
450	0.36 ±0.01	1.98 ±0.01	17.79 ±0.15	0.819 ±0.01	269.52 ±1.84	0.75 ±0.01	1651 ±14.88	1.71 ± 0.01
500	1.38 ±0.01	1.01 ±0.01	18.79 ±0.14	0.597 ±0.01	171.94 ±1.15	6.93 ±0.01	553.02 ±5.45	2.17 ± 0.01
550	1.21 ±0.01	0.59 ±0.01	10.13 ±0.06	0.469 ±0.01	47.07 ±0.29	0.85 ±0.01	103.60 ±0.44	3.21 ± 0.03
600	0.77 ±0.01	0.38 ±0.01	3.43 ±0.02	0.440 ±0.01	10.87 ±0.09	1.08 ±0.06	15.36 ±0.26	5.81 ± 0.09
650	0.42 ±0.01	0.26 ±0.01	0.98 ±0.01	0.53 ±0.01	2.25 ±0.02	1.58 ±0.02	2.22 ±0.02	13.77 ±0.33

Table 6.5: Values of the components for equivalent circuit model for BFT5 (x = 0.05)

Temp(K)	R_1(KΩ)	C_1(nF)	R_2(KΩ)	C_2(nF)	R_3(KΩ)	C_3(nF)	R_4(KΩ)	C_4 (nF)
300	0.86 ± 0.06	2.20 ± 0.07	64.07 ± 3.52	1.36 ± 0.03	4017.66 ± 190.14	0.82 ± 0.02	--	0.74 ± 0.01
350	0.95 ± 0.06	2.25 ± 0.07	84.99 ± 5.0	1.33 ± 0.03	4856.81 ± 209.7	0.69 ± 0.01	--	1.03 ± 0.03
400	0.76 ± 0.05	2.13 ± 0.06	109.84 ± 6.04	0.92 ± 0.02	3723.48 ± 98.46	5.09 ± 0.01	--	2.12 ± 0.09
450	0.26 ± 0.01	1.88 ± 0.01	17.45 ± 0.06	0.85 ± 0.01	470.82 ± 0.73	0.39 ± 0.01	1362.41 ± 2.93	1.01 ± 0.01
500	0.25 ± 0.01	1.29 ± 0.01	10.97 ± 0.09	0.55 ± 0.01	150.78 ± 0.51	0.31 ± 0.01	191.03 ± 0.69	1.88 ± 0.01
550	0.25 ± 0.01	0.89 ± 0.01	7.03 ± 0.08	0.34 ± 0.01	34.18 ± 0.11	0.34 ± 0.01	29.78 ± 0.15	3.41 ± 0.04
600	0.34 ±0.01	0.53 ± 0.01	4.53 ± 0.04	0.23 ± 0.01	5.36 ± 0.05	6.7 ± 0.14	6.79 ± 0.41	0.64 ± 0.01
650	0.23 ± 0.01	0.32 ± 0.01	1.70 ± 0.02	0.90 ± 0.02	1.60 ± 0.01	0.21 ± 0.01	1.17 ± 0.02	10.42 ± 0.31

The modulus data for the composition x = 0.10 were also analysed in the same way. M″ vs M ′ curves had appearance similar to those shown in Figures 6.7 (c) and 6.8 (c), passed through origin and did not possess a rising high frequency branch. These plots are not shown for brevity. The sample has predominant hexagonal phase with very small amount of tetragonal phase. Therefore, treating this also as a two phase system, an equivalent circuit model comprising four parallel RC circuits connected in series was considered where R_1C_1, R_2C_2, R_3C_3 and R_4C_4 represented hexagonal phase, tetragonal phase, grain boundary and sample-electrode interface respectively. The values of the components were obtained as discussed in the preceding paragraphs and are given in Table 6.6. The values of χ^2 (indicating the goodness of fit) for all the samples are below 0.05. The equivalent circuit models and the values of the components may be useful for simulation purposes.

Table 6.6: Values of the components for equivalent circuit model for BFT10 (x = 0.10)

Temp(K)	R_1(KΩ)	C_1(nF)	R_2(KΩ)	C_2(nF)	R_3(KΩ)	C_3(nF)	R_4(KΩ)	C_4 (nF)
300	1.27 ±0.04	0.52 ± 0.01	35.13 ±0.92	0.31 ±0.01	425.92 ±9.02	0.30 ±0.01	2543.28 ±24.29	0.53 ±0.01
350	0.91 ± 0.03	0.52 ± 0.01	20.64 ±0.63	0.37 ± 0.01	385.87 ±9.34	0.24 ±0.01	1127.95 ±12.85	0.58 ± 0.01
375	0.72 ± 0.03	0.46 ±0.01	13.44 ± 0.48	0.34 ±0.01	179.94 ±3.64	0.23 ±0.01	250.76 ±4.63	1.23 ± 0.05
400	0.62 ± 0.03	0.42 ±0.01	9.29 ± 0.42	0.30 ± 0.01	68.36 ± 1.14	0.26 ±0.01	56.22 ±1.60	2.89 ± 0.17
450	0.51 ± 0.04	0.35 ± 0.01	5.31 ±0.37	0.26 ± 0.01	14.75 ±0.34	0.39 ±0.01	9.62 ± 0.44	7.31 ± 0.68
500	0.22 ± 0.03	0.26 ± 0.04	3.82 ± 0.16	0.35 ± 0.02	1.45 ±0.11	0.29 ±0.02	1.96 ± 0.15	3.82 ± 0.32

6.3.5 Dielectric characterization (Microwave Range)

Variations of dielectric constant and dielectric loss in the frequency range 8 – 12 GHz (X-Band) measured at room temperature are shown in Figure 6.9. The permittivity values are in the range 17.5 – 19.5 over the whole frequency range 8 – 12 GHz for BFT3 and BFT5 while it is in the range 15.5-17.6 for BFT10. It is to be noted that the room temperature permittivity values at 1 MHz are 50, 500 and 66 for BFT3, BFT5 and BFT10 respectively as discussed in section 6.3.3 where the higher value for BFT5 was attributed to the larger interfacial regions between tetragonal and hexagonal phases created due to formation of more hexagonal grains in this composition. The values decrease for all the compositions in the X- Band range. This is reasonable as interfacial and space charge polarizations cease to respond at microwave frequencies and the contribution to permittivity comes mainly from atomic and electronic polarizations. These are lossy dielectric materials which may be used in developing antennas with enhanced bandwidth by loading [Zivkovic (2012)].

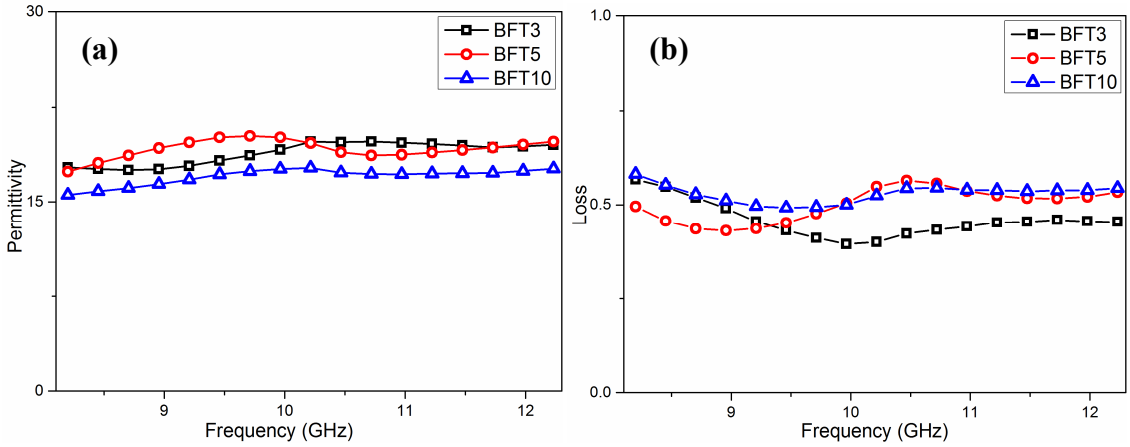

Figure 6.9: (a) Permittivity vs. frequency and (b) loss vs. frequency plots for $BaFe_xTi_{1-x}O_3$ for x = 0.03, 0.05 and 0.10 in X-Band.

6.4 Conclusion

Compositions with x = 0.03, 0.05 and 0.10 were prepared in the system $BaFe_xTi_{1-x}O_3$ by solid state reaction method and characterized by using XRD , SEM and EDX. It was found that these samples contain both tetragonal and hexagonal phases, the latter increasing as the doping level is raised. Spherical grains are observed for the sample with x=0.03 while the composition with x=0.05 has mixed rectangular and rod-like grains. Only rod-like grains are observed in the sample with x=0.10. Composition with x=0.03 exhibits a behavior which mimics relaxor ferroelectrics. Sample with x=0.05 shows diffuse phase transition. Contributions of tetragonal and hexagonal phases, grain boundary and electrode to the overall dielectric behavior have been separated using complex plane modulus analysis and equivalent circuit models representing the data well were developed. The values of dielectric permittivity measured in the frequency range 8-12 GHz in the X band of microwaves are around 16-20 for all the samples and are almost independent of frequency with the loss being around 0.5.